CrossMark

Activated carbon fibers for efficient VOC removal from diluted streams: the role of surface functionalities

Guillaume B. Baur[1] · Oliver Beswick[1] · Jonathan Spring[1] · Igor Yuranov[1] · Lioubov Kiwi-Minsker[1]

Abstract The effect of surface functionalities, specific surface area and pore size of activated carbon fibers (ACFs) on the adsorption of toluene and acetaldehyde, two volatile organic compounds (VOC), at low concentrations (~80 ppmv) and short contact time (20 ms) has been studied. Two different types of ACFs characterized by low temperature N_2 adsorption: ultramicroporous ($d_{pore} < 1$ nm) and supermicroporous ($d_{pore} \sim 1$–2 nm) were tested. Both ACFs were effective for the removal of toluene attaining the adsorption capacity as large as 51 wt%. The surface chemistry of ACFs (O-containing functional groups) was characterized by temperature-programmed desorption monitoring the CO/CO_2 evolved. Oxidative treatment of ACFs by nitric acid increased the surface concentration of O-groups. This resulted in lower adsorption capacity towards toluene but higher one towards acetaldehyde. This result was rationalized based on different type of VOC interactions with the carbon surface.

Keywords Activated carbon fibers · Microporosity · Adsorption · Volatile organic compounds

1 Introduction

Contamination of the environment by anthropogenic volatile organic compounds (VOC) has become a great issue during the last decades (Foster et al. 1992; Cal et al. 1997; Popescu et al. 2003; Lillo-Rodenas et al. 2005). Present in gas streams of many industrial exhausts (Piccot et al. 1992), they are harmful and detrimental even at low concentrations (<100 ppmv) (Tancrede et al. 1987; Ruhl 1993; Wu et al. 2009).

Several techniques have been developed and applied for VOC abatement e.g.: absorption, adsorption, condensation, photo-, thermal or catalytic oxidation (Ruddy and Carroll 1993; Li et al. 2011; Okubo et al. 2001; Mo et al. 2009). Adsorption appears to be the most efficient method for complete removal of VOC from diluted streams. Various adsorbents are used for VOC abatement, such as activated carbons (AC) (Lillo-Rodenas et al. 2005), zeolites (Huang et al. 2006; Datka 1981), silica (Hernandez et al. 2004) and polymers (Choung et al. 2001). Among them, AC shows the most promising results (Hayashi et al. 2006; Lillo-Rodenas et al. 2005; Park et al. 2010) due to low cost and versatility to different compounds. AC are usually used in the form of granules, powder, pellets or fibers (Park et al. 2007; Romero-Anaya et al. 2010; Mohan et al. 2009; Lillo-Rodenas et al. 2011). Consisting of arranged microfilaments with high specific surface area (SSA), activated carbon fibers (ACFs) demonstrate fast adsorption kinetics, suppressed mass transfer limitations and lower pressure drop as compared to randomly packed beds (Singh et al. 2002; Das et al. 2004).

Despite the wealth of information available in the literature concerning VOC abatement using ACFs, studies of adsorption dynamics at low VOC concentrations (<200 ppmv) are scarce (Foster et al. 1992; Lillo-Rodenas et al. 2011; Dimotakis et al. 1995). Moreover, most of them deal with lower gas linear velocities (<0.1 m s^{-1}) as compared to ones of industrial waste streams.

The present study investigates ACFs towards toluene and acetaldehyde adsorption at very low concentrations (<100 ppmv) and short contact time (~20 ms). Adsorption dynamics on

✉ Lioubov Kiwi-Minsker
  lioubov.kiwi-minsker@epfl.ch

[1] Group of Catalytic Reaction Engineering, Ecole Polytechnique Fédérale de Lausanne, EPFL-SB-ISIC-GGRC, Station 6, 1015 Lausanne, Switzerland

two different commercial microporous ACFs were studied by a transient response method (Wagner and Hauffe 1938, 1939; Tamaru 1964). This methodology was originally developed for kinetic studies of catalytic reactions but is easily adapted for adsorption. It is based on monitoring of response at the tubular reactor outlet on a quick change of concentration at the reactor inlet. "Dynamic column method" is used to measure the adsorption capacity. This method requires a constant VOC flow through a sorbent bed and a continuous monitoring of the downstream concentration. In this way breakthrough curves are usually obtained. The adsorption capacity is calculated by numerical integration of the area defined between the breakthrough curve of the inert tracer and the adsorbate (Pei and Zhang 2012).

It is known that the adsorption capacity of AC towards VOC is governed by both surface morphology [pore size, SSA (Mangun et al. 1998)] and surface functional groups (Lillo-Rodenas et al. 2005). An oxidative treatment by nitric acid was applied to modify the surface morphology and to increase the concentration of O-containing groups on ACFs surface (Bulushev et al. 2004). A systematic characterization of the SSA, pore size and O-content was carried out in order to quantify the effect of these variables on the adsorption capacity towards toluene and acetaldehyde.

2 Experimental

2.1 Setup

The setup used for adsorption study via transient response method is shown in Fig. 1. It consists of a gas generator (FlexStream Base Permeation Unit), two pneumatic actuators connected to a spool valve (Asco Numatics), a quartz tubular reactor (length 25 cm, inner diameter 3 mm) and a sensitive mass spectrometer (Hiden Analytical HPR 20 QIC). The reactor charged with an adsorbent is placed in a tubular oven (Carbolite MTF 10/25/130) for temperature control.

Pressurized air (6 bar) was connected to a spool valve (solenoid air pilot operated-spring return) controlled with a numerical unit (National Instrument 6009) equipped by the LabView software. Depending on the spool valve position, pressurized air is directed to one of the two outlets and then to both pneumatic actuated three-way valves (Whitey, double acting mode, 180° actuation) via ¼ inches stainless steel tubing. The position of the pneumatic actuated three-way valves (i.e. reactor or bypass line) depends on which pneumatic actuator inlet was under pressure. Due to the pressure, a piston in the actuator chamber moves from one position to another creating an inversion of the connected three-way valves. To insure simultaneous switch of both three-way valves,

tubes length between the spool valve and both pneumatic actuators are identical. With the described valves system, the switch from the bypass to the reactor line or inversely was reproducible and sufficiently quick to avoid any disturbance of the gas flow.

The gas generator providing a diluted toluene or acetaldehyde (ppm, ppb) flow was composed of a gas line with a mass flow controller connected to a permeation tube and an oven. A permeation tube with a calibrated permeation membrane filled with liquid toluene (99.9 % VWR Chemicals, AnalaR NORMAPUR) or acetaldehyde (99.5 % Sigma–Aldrich, Fluka Analytical) was placed in the oven at desired temperature. Thus, the adsorbate permeation rate was controlled by the oven temperature (303–353 K $\pm$ 0.01 K). Its concentration (10–100 ppmv) was adjusted at a fixed flow rate (100–1000 cm^3 min^{-1}).

The reactor outlet was continuously monitored by an online mass spectrometer with short sampling time (<500 ms), high sensitivity (500 ppb) and stability (<$\pm$0.5 % variation over 24 h).

2.2 Materials

Activated carbon fibers were purchased from Kynol Europa GmbH (Hamburg, Germany). They are produced from Kynol novoloid (phenolic) precursor fibers by a one-step process combining both carbonization and chemical activation. Two types of samples were used, namely: ACF-1 (SSA $\sim$1000 m^2 g^{-1}) and ACF-2 (SSA $\sim$2000 m^2 g^{-1}).

All gases, helium (99.999 %), nitrogen (99.999 %) and the mixtures: argon 2 % v/v Ar/He, 3 % v/v CO/He and 2 % v/v CO$_2$/He were provided by Carbagas (Switzerland).

The HNO$_3$ treated ACF-2 were prepared by an immersion of original ACF-2 in a boiling 15 % (vol/vol) aqueous solution of nitric acid (HNO$_3$ 65 vol%, VWR chemicals, AnalaR NORMAPUR) for different time (1, 15 and 30 min) followed by a rinsing with demineralized water and drying in ambient air. The abbreviations for the samples are as following: ACF-2/HNO$_3$-30m means the ACF-2 samples treated by HNO$_3$ for 30 min.

2.3 ACFs characterization

Specific surface area and pore size distribution were determined by physical adsorption of N$_2$ at 77 K using a Sorptomatic 1990 (Carlo Erba Instruments). Prior to analysis, original samples and oxidized ones were outgassed at 523 K for 2 h under vacuum (7 $\times$ 10^{-2} bar) and at 373 K for 3 h under vacuum (7 $\times$ 10^{-2} bar) respectively. N$_2$ adsorption/desorption isotherms were measured over the relative pressure range 0.0005 $\leq$ P/P$_0$ $\leq$ 0.98. The total pore volume and the specific surface area were obtained using the BET method (Brunauer et al. 1938).
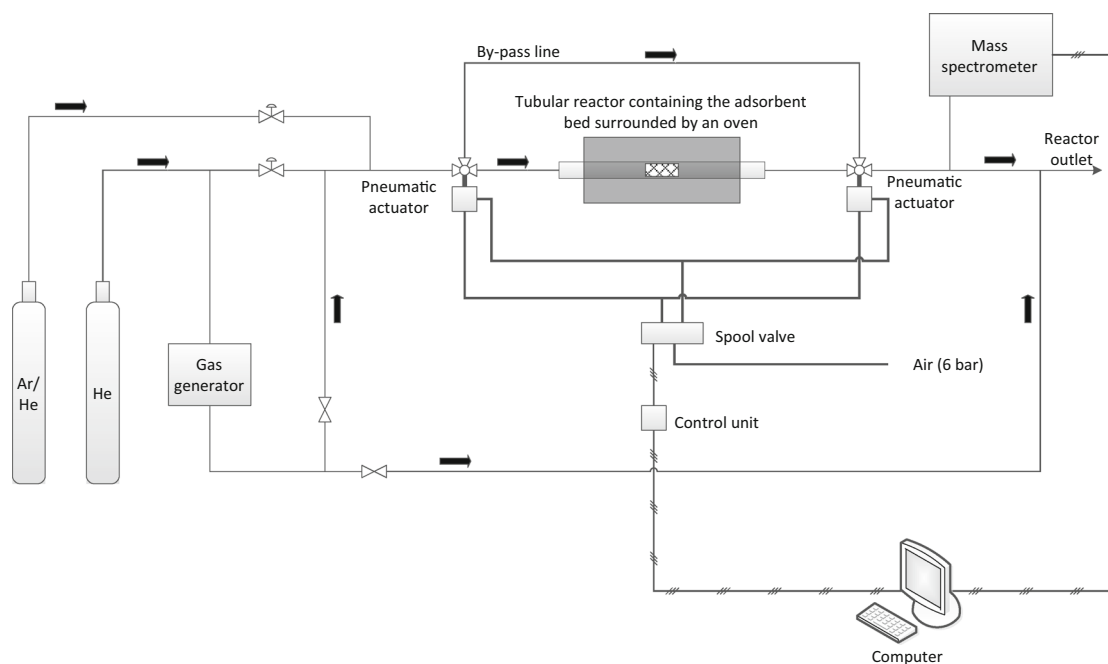
Fig. 1 Scheme of the setup for adsorption study

The characterization and quantification of oxygen-containing groups on the ACFs surface were performed via TPD experiments. An ACFs sample ($\sim$100 mg) loaded in a quartz reactor connected to a mass spectrometer was heated in a He flow (100 cm^3 min^{-1}) up to 1223 K (temperature ramp 10 K min^{-1}). Prior to the experiment, the reactor was purged by He for 30 min at room temperature. The gases evolved from the ACFs sample (CO and CO$_2$) due to decomposition of O-containing groups were analyzed via the calibrated mass spectrometer and the concentration profiles were integrated. Water and NO were also detected below 673 and 473 K respectively in negligible amounts. The low amount of water was attributed to physisorbed molecules whereas traces of NO were probably coming from HNO$_3$ remaining after rinsing.

Scanning electron microscopy (SEM) was carried out using a Carl Zeiss MERLIN FE-SEM equipped with two, annular and Everhart–Thornley secondary-electron (SE), detectors operated at an accelerating voltage of 5–30 keV with a beam current of 1.0–3.0 nA and using Zeiss Smart SEM software for data acquisition/manipulation.

2.4 Dynamic adsorption measurements

Before measurements, the ACFs samples (10 ± 0.1 mg) placed in the central part of the quartz tubular reactor were outgassed at 298 K in a He flow (40 cm^3 min^{-1}). The adsorption experiments were carried out at 298 ± 1 K and with gas flow rate of 300 cm^3 min^{-1} (linear velocity 0.5 m s^{-1}). The gaseous mixtures contained 80 ppmv of toluene or acetaldehyde in He. The inert tracer signal (Ar 2 %v/v in He) was obtained independently.

The adsorption capacity measurements consist of the following steps:

1. Stabilization of the gas mixture (VOC in He) flow through the bypass to measure the initial VOC concentration.

2. After a switch to the reactor, the gas mixture flows through the adsorbent bed until the outlet VOC concentration reaches the initial one measured during the stabilization step. In such a manner a breakthrough curve was obtained.

The Argon breakthrough curve was measured to characterize the flow pattern and the residence time distribution in the reactor. The Ar–He mixture was injected through the reactor pre-purged by He, using a switch from the bypass to the reactor line.

The area defined between the Ar and the VOC breakthrough concentration curves was numerically integrated and the adsorption capacities (wt%) were obtained.

3 Results and discussion

3.1 Characterization of ACFs adsorbents

3.1.1 Morphology

The ACFs materials consist of elementary filaments of $\sim$10 μm diameter. The representative SEM image of the

adsorbents is shown in Fig. 2. Figure 3 presents typical N_2 adsorption isotherms over the samples used in this study and indicates larger nitrogen adsorption capacity of the ACF-2 as compared to ACF-1. All isotherms exhibit a type I profile typical for microporous adsorbents according to the IUPAC classification (Sing et al. 1985). As shown in Fig. 3 the nitric acid treatment decreases the pore volume while keeping similar N_2 adsorption curve shape indicating that the material remains microporous despite oxidative treatment. A gradual decrease of the porosity can be obtained by increasing the nitric acid treatment time.

In order to evaluate more precisely the morphology of the ACF-1, ACF-2 and the nitric acid treated samples, a pore size determination was carried out via comparative α-method (Sing 1968). The α-plot is a widely used method for characterization of porous adsorbents. It is based on the comparison of the N_2 adsorption isotherms between a chemically similar nonporous reference adsorbent and the studied adsorbents. This comparison is based on the assumption that the surface properties of the reference and the studied solids are very similar. In this work, carbon black was chosen as a non-porous reference material. Normalizing the N_2 amount adsorbed onto the nonporous reference at different partial pressure by the amount adsorbed at $p/p^0 = 0.4$ gives the α_s reference. The amount adsorbed onto the studied adsorbent is then plotted against α_s at the corresponding relative pressure. Depending on the shape of the α-plot, the porosity of different samples can be compared (Carrott et al. 1987).

The α-plots obtained for all ACFs samples (Fig. 4) are almost linear and constant at $\alpha > 1$. This implies that the external surface area is relatively small as compared to the total surface area meaning that most of the surface is due to the pores (Rouquerol et al. 1999). It confirms that both
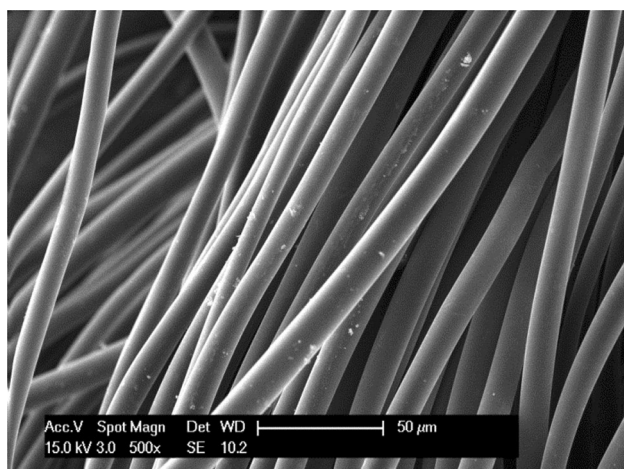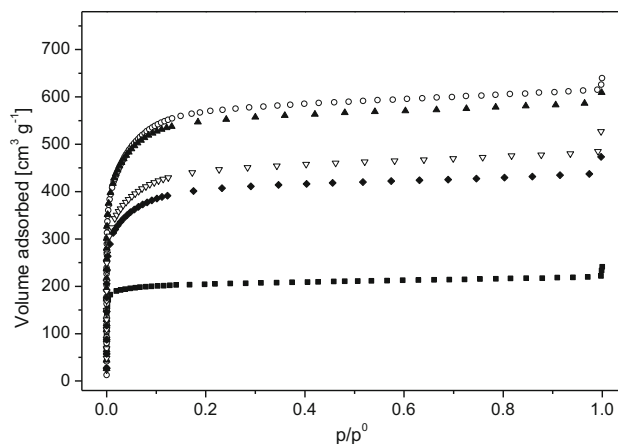
Fig. 3 Nitrogen adsorption isotherms for ACF-1 (*filled square*), ACF-2 (*circle*), ACF-2/HNO$_3$-1 m (*filled triangle*), ACF-2/HNO$_3$-15 m (*inverted triangle*) and ACF-2/HNO$_3$-30 m (*filled diamond*)
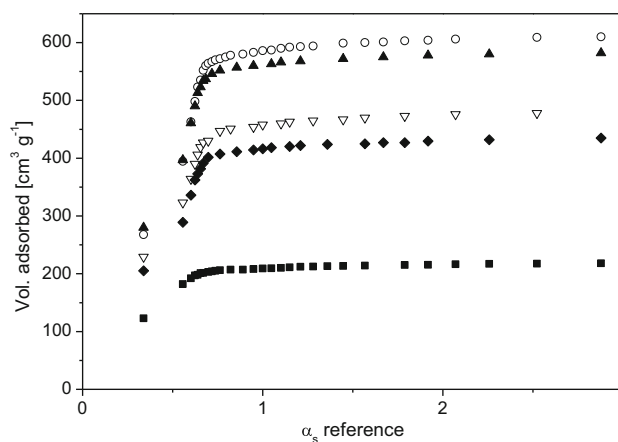
Fig. 4 α-plot of ACF-1 (*filled square*), ACF-2 (*circle*), ACF-2/HNO$_3$-1 m (*filled triangle*), ACF-2/HNO$_3$-15 m (*inverted triangle*) and ACF-2/HNO$_3$-30 m (*filled diamond*)

adsorbents are microporous with the relatively narrow pore size distribution.

The curve slope is changing for all materials in the range of $0.5 < \alpha_s < 1$. The slope change of ACF-1 appears at $\alpha_s \sim 0.6$ whereas an extremely steep slope is observable at slightly higher α_s values for ACF-2. The α value difference at which the slope change occurs is interpreted as a microporosity difference between ACF-1 and ACF-2. A slope change at higher α_s values (ACF-2) signifies relatively large micropores (Almazan–Almazan et al. 2009). It is then suggested that ACF-2 contains mainly supermicropores whereas ACF-1 is an ultramicroporous adsorbent. Since the α-plot slope change occurs at identical value for ACF-2 and ACF-2 treated by nitric acid, it is concluded that nitric acid treatment does not affect the micropore diameter while decreasing the total pore volume.

Fig. 2 SEM image of ACF-2

Table 1 Characteristics of ACFs adsorbents

Sample	SSA$_{BET}$ (m^2 g^{-1})	C	Pore volume (cm^3 g^{-1})
ACF-1	800	6400	0.4
ACF-2	2170	280	1.0
ACF-2/HNO$_3$-1 m	2100	400	1.0
ACF-2/HNO$_3$-15 m	1670	370	0.9
ACF-2/HNO$_3$-30 m	1530	420	0.8

The specific surface area of all samples was calculated through the BET equation using N$_2$ adsorption data (Brunauer et al. 1938). The equation was linearized in the partial pressure range of 0.001–0.07 for ACF-1 and 0.01–0.1 for ACF-2 and ACF-2/HNO$_3$ (all treatment times). As shown in Table 1, the C values obtained are >100 for all the samples confirming their microporous morphology. The C value of the BET equation which can qualitatively describe the pore size, remained constant for original and nitric acid treated ACF-2 signifying a constant micropore size and confirming the interpretation of the α-plot. Similar results were already obtained for oxidized activated carbon (Pradhan and Sandle 1999; Dimotakis et al. 1995; Salame and Bandosz 1999). On the opposite, ACF-1 is characterized by a larger C value as compared to ACF-2 and ACF-2/HNO$_3$ indicating narrower microporosity. The micropore volume of the original ACF-2 is larger as compared to ACF-1. Therefore HNO$_3$ treatment was found to reduce both the SSA and pore volume of ACF-2 while keeping its micropore structure (Fig. 4).

3.1.2 Surface functionalities

O-containing groups on the ACFs surface were characterized by temperature-programmed desorption (TPD) with the outlet composition monitored by MS. Two major molecules desorbing from the ACFs surface are CO and CO$_2$ although traces of H$_2$O and NO were detected. CO$_2$ is assumed to originate from decomposition of carboxylic (373–673 K), lactone (463–923 K) and anhydride groups (623–900 K), whereas CO is a product of decomposition of anhydride (623–900 K) phenolic (873–973 K), carbonyl (973–1173 K) and quinone groups (973–1173 K) (Figueiredo et al. 1999).

Figure 5 shows TPD profiles of original and oxidized samples. As can be seen, treatment of ACF-2 by nitric acid increases drastically the surface oxygen content. Even a short treatment time (1 min) in boiling nitric acid leads to a large increase in surface oxygen content. All type of surface O-containing groups is created by such treatment. Anhydride groups are identified by the broad shoulder at 800 K on both CO and CO$_2$ desorption pattern. As compared to the other desorption peaks, the quantity of anhydride groups is relatively low. Particularly visible on the ACF-2/HNO$_3$-1 m pattern, the CO decomposition peaks at
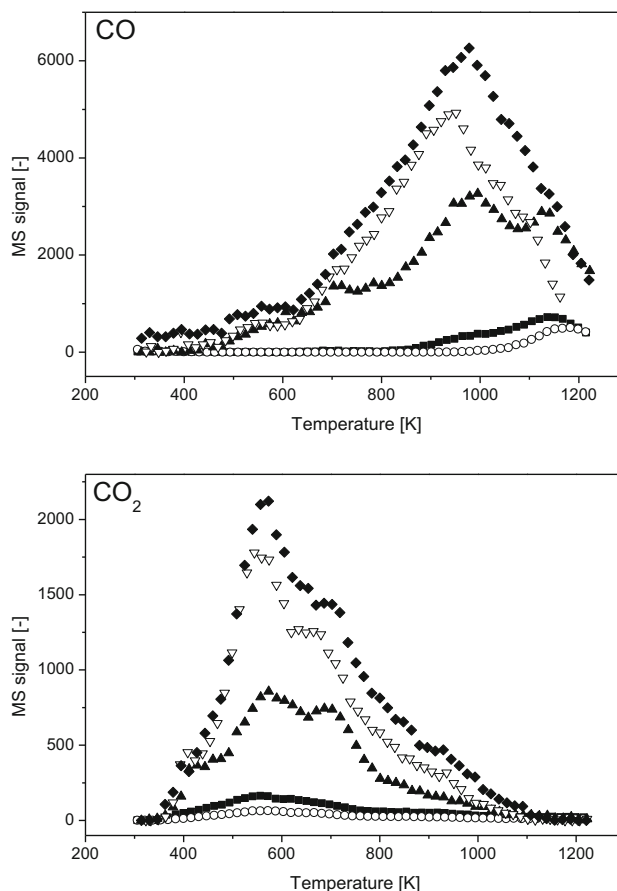
Fig. 5 TPD profiles of ACF-1 (*filled square*), ACF-2 (*circle*), ACF-2/HNO$_3$-1 m (*filled triangle*), ACF-2/HNO$_3$-15 m (*inverted triangle*) and ACF-2/HNO$_3$-30 m (*filled diamond*)

1000 and 1150 K indicate the creation by the oxidative treatment of phenolic and carbonyl or quinone groups respectively. For longer treatment time, due to the higher amount of groups created, the two decomposition peaks are not distinguishable. The CO$_2$ decomposition pattern of all the oxidized samples revealed that carboxylic groups are created in a large amount although a small amount was already present on both original samples (550 K). Decomposing at higher temperature (700 K), lactone groups are created by the oxidative process in a smaller extent.

The integration of the CO and CO$_2$ concentration curves gives the surface oxygen content of the samples which are

Table 2 Quantitative characterization of ACFs surface oxygen groups

Sample	CO$_2$ (μmol/g$_{ACFs}$)	CO (μmol/g$_{ACFs}$)	Total oxygen content (μmol/g$_{ACFs}$)
ACF-1	470	330	800
ACF-2	240	180	420
ACF-2/HNO$_3$-1 m	2200	2800	5000
ACF-2/HNO$_3$-15 m	4000	3500	7500
ACF-2/HNO$_3$-30 m	4000	4200	8200

reported in Table 2. For original and nitric acid treated samples the amount of evolved CO is comparable to the amount of CO$_2$ indicating that all type of O-containing groups are present on the ACFs surface. However, the total oxygen concentration in the original ACFs was found to be quite low and comparable to previously published results (Lillo-Rodenas et al. 2005, 2011). As shown in Fig. 5, ACF-1 contains more O-containing groups decomposing in CO$_2$ as compare to ACF-2. The amount of CO evolved is also slightly higher in the case of ACF-1. Therefore, the concentration of polar groups on the ACF-1 surface is larger. Nitric acid treatment increased considerably the oxygen content in ACF-2. Indeed, ACF-2/HNO$_3$-30 m has 20 times more surface O-containing groups as compared to the original ACF-2.

3.2 Reactor flow pattern

The characterization of the tubular reactor used for adsorption experiment is carried out using the dispersion model. The dimensionless group used to characterize the residence time distribution in the real tubular reactor is the vessel dispersion number:

$$\frac{D_{ax}}{uL} \tag{1}$$

where D_{ax} is an axial dispersion coefficient, u is a linear velocity in the reactor and L is a length of the reactor.

If this number tends to 0, the dispersion is negligible, hence a plug flow behavior can be assumed. A vessel dispersion number tending to infinite means a large dispersion or a complete back-mixing behavior. In practical cases 0.01 is the threshold value under which a tubular reactor can be treated as ideal plug flow.

In this study, the vessel dispersion number was obtained using step-wise injection of an inert tracer (Argon) into He flow through the reactor. Different gas flow rates were applied. The Ar concentration at the reactor outlet was monitored by the mass spectrometer (Fig. 6).

The mean residence time, $\bar{t}$, and the variance around the mean, σ^2, are subsequently calculated:

$$\bar{t} = \int_0^1 t\,dF = \sum_0^1 t_i \Delta F_i \tag{2}$$
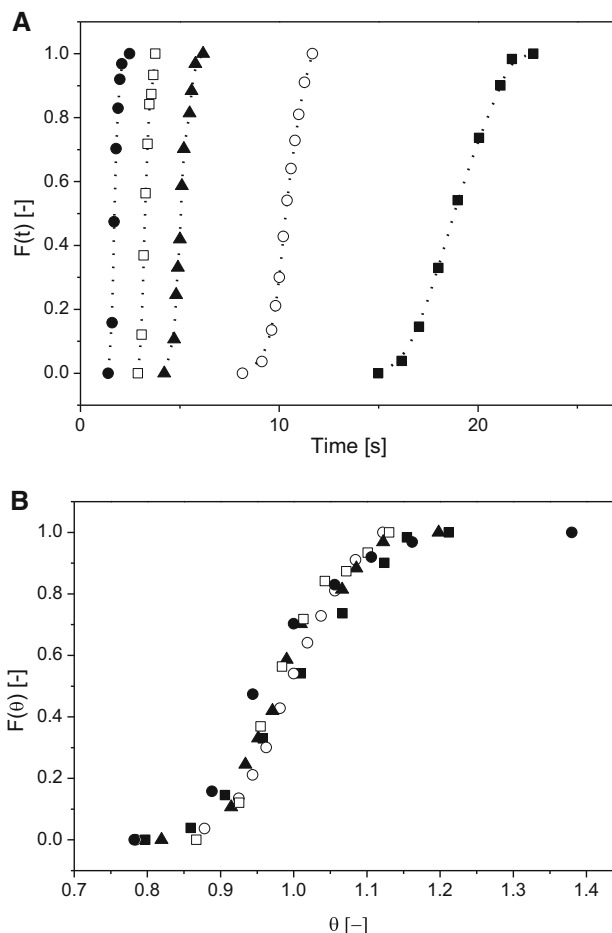
Fig. 6 Reactor outlet response to a step-wise injection of Ar (inert tracer) at the reactor inlet as function of time (**a**) and dimensionless time (**b**) at different flow rate: 25 cm^3 min^{-1} (*filled square*) 50 cm^3 min^{-1} (*circle*), 100 cm^3 min^{-1} (*filled triangle*), 200 cm^3 min^{-1} (*square*), 400 cm^3 min^{-1} (*filled circle*)

$$\sigma^2 = \int_0^1 (t - \bar{t})^2\,dF = \sum_0^1 (t_i - \bar{t})^2 \Delta F_i \tag{3}$$

ΔF_i was obtained by normalizing the tracer concentration:

$$F(t) = \frac{c_i}{c_0} \tag{4}$$

where c_o is an inlet Ar concentration and c_i is a concentration at time t.

Table 3 Dispersion number as a function of gas flow rate

Flow rate ($cm^3 min^{-1}$)	Dispersion number $\left(\frac{D_{ax}}{L_t u}\right)(-)$
7.5	0.0122
10	0.0087
25	0.0034
50	0.0023
100	0.0019
200	0.0025
400	0.0040

The vessel dispersion number for small extents of dispersion was obtained by combining Eqs. (2) and (3):

$$\sigma_\theta^2 = \frac{\sigma^2}{\bar{t}^2} = 2\left(\frac{D}{uL}\right) \tag{5}$$

The obtained values are presented in Table 3. It can be seen that for all flow rates >10 ml min^{-1} the vessel dispersion number is <0.01. A "piston type" flow pattern is therefore insured at all flow rates. Presented in Fig. 6b the rector response to a stepwise injection normalized by its mean residence time shows that identical flow pattern is obtained for all the flow rate tested.
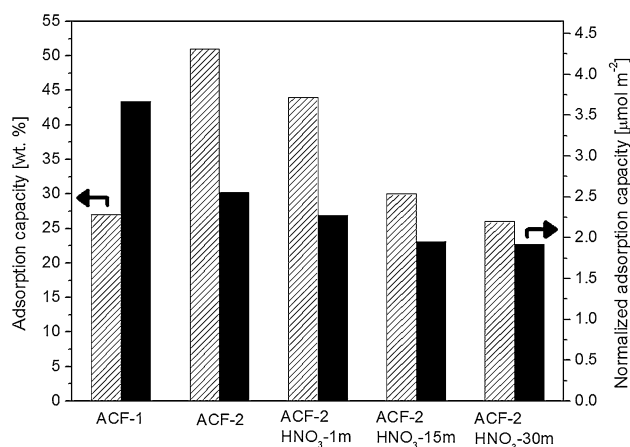
3.3 Toluene adsorption

Toluene breakthrough curves are shown in Fig. 7. The adsorption capacity of the ACFs materials was determined by a numerical integration of the area defined by the adsorbate concentration curve and the argon curve between t_0 and t_{final} when the outlet concentration is equal to the inlet one.

As shown in Fig. 7, ACF-2 is efficient for toluene adsorption even at short contact time (~ 20 ms). The outlet
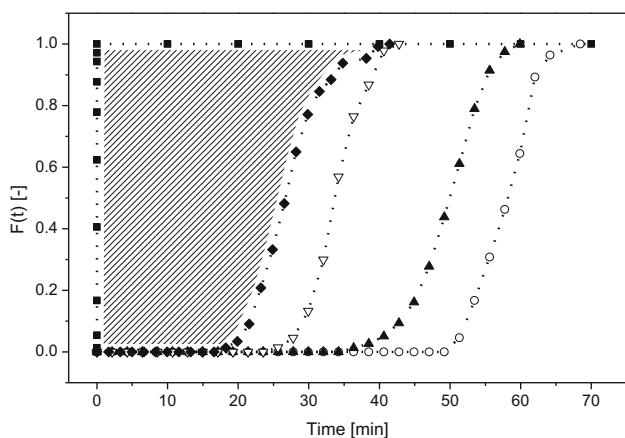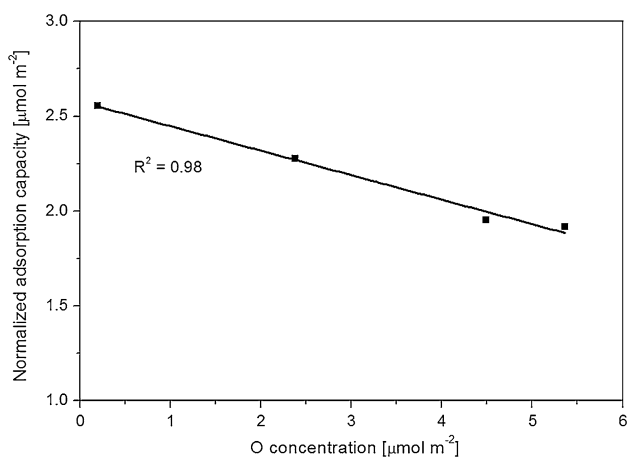
Fig. 8 Toluene adsorption capacities as a function of nitric acid treatment

toluene concentration is zero indicating its total adsorption before the breakthrough at about 50 min. The toluene adsorption capacity obtained is 51 wt%. This value is in agreement with already published results (Lillo-Rodenas et al. 2011).

The modification of ACF-2 by nitric acid gradually decreases the toluene adsorption capacity with the HNO$_3$ treatment time (Fig. 8). From 51 wt% for original ACFs the adsorption capacity drops to 44, 30 and 26 wt% for ACF-2/HNO$_3$-1 m, ACF-2/HNO$_3$-15 m ACF-2/HNO$_3$-30 m respectively. The breakthrough curve shape of the oxidized samples is identical to the original sample suggesting similar adsorption kinetics. This observation can be explained by the constant micropore size upon nitric acid treatment (Fig. 4). The adsorption kinetics, usually governed by internal mass transfer, is therefore identical (Fournel et al. 2010). The lower adsorption capacity of the HNO$_3$ treated ACFs is explained by their lower SSA (Table 1) and higher oxygen contents (Table 2). It is known that a lower specific surface area leads to a lower adsorption capacity for similar pore sizes (Lillo-Rodenas et al. 2011), whereas O-containing groups weaken the interaction between benzene ring of toluene molecules and graphite layers of ACFs (Lillo-Rodenas et al. 2005). To quantify both effects, the adsorption capacity is normalized by the SSA of the adsorbent. The normalized efficiencies reflect the effect of the O-containing groups. It decreases with nitric acid treatment (Fig. 8). It is then concluded that the presence of O-containing groups decreases the adsorption capacity.

To quantify the effect of the O-containing groups, the adsorption capacity normalized by the SSA of the different samples is plotted on the oxygen surface concentration. The results presented in Fig. 9 show a linear trend, confirming that polar groups weaken the interaction between toluene and ACFs surface.

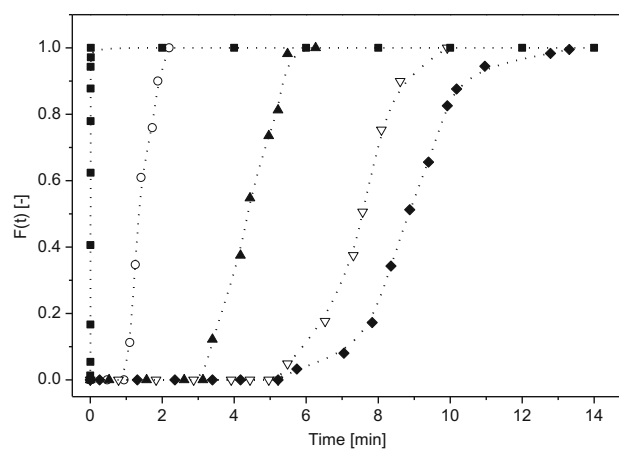**Fig. 7** Toluene (80 ppmv) breakthrough curves for ACF-2 (*circle*), ACF-2/HNO$_3$-1 m (*filled triangle*), ACF-2/HNO$_3$-15 m (*inverted triangle*), ACF-2/HNO$_3$-30 m (*filled diamond*) and 2 % (v/v) Argon (*filled square*). Total flow rate (STP) 300 cm^3 min^{-1} (298 K)

Fig. 9 SSA normalized adsorption capacity towards toluene as function of the O-concentration of ACF-2

Fig. 10 Acetaldehyde (80 ppmv) breakthrough curves for ACF-2 (*circle*), ACF-2/HNO$_3$-1 m (*filled triangle*), ACF-2/HNO$_3$-15 m (*inverted triangle*), ACF-2/HNO$_3$-30 m (*filled diamond*) and 2 % (v/v) Argon (*filled square*).Total flow rate (STP) 300 cm^3 min^{-1} (298 K)

The effect of the ACFs microporosity on toluene adsorption capacity was studied by comparing ACF-1 and ACF-2 (Fig. 8). As discussed above, ACF-1 micropores are narrower as compared to ACF-2 ones. The toluene adsorption capacity obtained was 27 wt% for ACF-1 and 51 wt%, for ACF-2. The adsorption capacities normalized by the SSA were 3.53×10^{-6} and 2.55×10^{-6} mol m^{-2}, respectively. The value found for ACF-1 is out of the trend shown in Fig. 8. Despite higher surface oxygen concentration (1 μmol m^{-2}) the normalized adsorption capacity of ACF-1 is larger as compared to ACF-2. This result is explained by the pore size which is smaller for ACF-1. The shorter distance between the pore walls in ACF-1 results in a stronger adsorption of toluene molecules and denser occupation of the available carbon surface.

3.4 Acetaldehyde adsorption

The effect of ACFs surface functionalities on the acetaldehyde adsorption was studied using the same adsorbents and the method described in Sect. 3.3. At similar concentration (80 ppmv) a much lower acetaldehyde adsorption capacities were measured for the initial ACF-1 and ACF-2: 0.7 and 0.3 wt%, as compared to toluene adsorption: 26 and 51 wt%, respectively. Despite their lower adsorption capacity, the breakthrough curves in Fig. 10 are showing a complete acetaldehyde removal. Moreover the steepness of the breakthrough curves insure fast adsorption kinetics. Similarly to toluene, the modification of the fibers by oxidative treatment does not influence the adsorption kinetics but only the total adsorption capacity. Low adsorption capacity towards acetaldehyde was already reported qualitatively for activated carbon (El-Sayed and Bandosz 2001) and activated carbon fibers (Dimotakis et al. 1995). Similarly to previously published results, oxidized samples demonstrated larger acetaldehyde adsorption capacities.

The O-containing groups of the activated carbon surface were suggested to enhance the acetaldehyde adsorption as compared to original ACFs.

The adsorption capacity as a function of the oxygen surface concentration is presented in Fig. 11 showing its proportionality to the oxygen surface concentration. Higher adsorption capacity is obtained for larger O-concentration hence, samples treated longer time by nitric acid shows larger adsorption capacity. Since all types of oxygen functionalities are created by the nitric acid treatment, it is not possible to indicate which surface oxygen containing groups contribute the most to the acetaldehyde adsorption. Figure 11 also shows that at higher acetaldehyde partial pressure the adsorption capacity increases for similar O-concentration. The acetaldehyde adsorption seems to involve the surface O-groups of the ACFs. The acetaldehyde adsorption mechanism on surface functional groups of activated carbon has been already reported (El-Sayed and Bandosz 2001). It is suggested that the aldehyde group of acetaldehyde interacts with O-containing groups of activated carbon via hydrogen bonding. The results presented in Fig. 11 are consistent with this mechanism.

The amounts of acetaldehyde adsorbed per gram are around 10 times lower than the O-content. They are between 0.07 and 0.5 μmol as compared to 0.4–8 μmol per gram of adsorbent of acetaldehyde and oxygen respectively. The coverage of the active sites by acetaldehyde remains relatively low at working partial pressure of 80 ppmv. The surface coverage by acetaldehyde is increasing with increase in the acetaldehyde partial pressure confirming that the maximum adsorption capacity is not reached at the working pressure.

The influence of the microporosity on acetaldehyde removal was also studied by comparing the adsorption
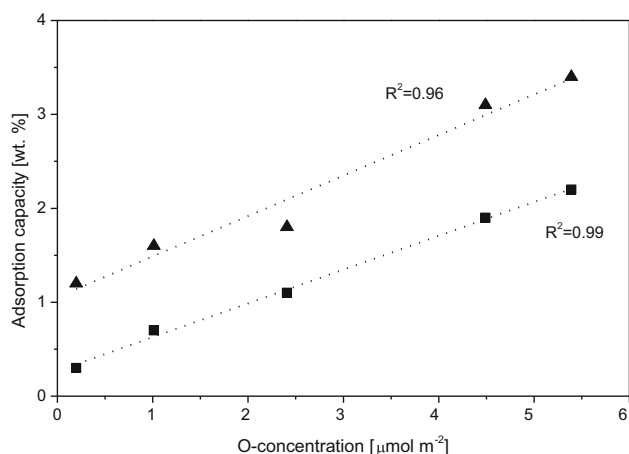
Fig. 11 Acetaldehyde adsorption capacity as a function of oxygen surface concentration for original ACF-1 and ACF-2 and HNO₃ treated ACF-2 (*filled square*). 80 ppmv acetaldehyde, (*filled triangle*) 150 ppmv acetaldehyde

capacity of ACF-1 and ACF-2. Although ACF-1 has smaller pore than ACF-2, the adsorption capacity of ACF-1 fits the trend shown in Fig. 11. This result suggests that the surface O-groups concentration is the key parameter controlling the acetaldehyde adsorption.

4 Conclusions

Adsorption of toluene and acetaldehyde VOC was studied by transient response method at low partial pressure (80 ppmv) and short contact time (~ 20 ms). Microporous activated carbon fiber materials ACFs were shown to be efficient for total toluene removal attaining the capacity as large as 51 wt%. Temperature-programmed desorption revealed that oxidative treatment by HNO₃ of the ACFs increased the surface concentration of O-containing groups. Toluene and acetaldehyde normalized adsorption capacities were shown to strongly depend on the surface functionalities. Larger surface O-concentration increases acetaldehyde removal but decreases the one of toluene. This effect was rationalized by suggesting a different type of interaction with the activated carbon surface. Acetaldehyde is adsorbed via hydrogen bonding with the O-containing groups while toluene adsorption is controlled by (ultra) microporosity.

References

Almazan-Almazan, M.C., Perez-Mendoza, M., Fernandez-Morales, I., Domingo-Garcia, M., Lopez-Garzon, F.J., Martinez-Alonso, A., Suarez-Garcia, F., Tascon, J.M.D.: Narrow microporosity characterization in polyaramid-derived carbons by adsorption of N₂, CO₂ and organic vapours. In: Kaskel, S., Llewellyn, P., Rodriguez-Reinoso, F., Seaton, N.A. (eds.) Characterisation of Porous Solids Viii. Royal Society of Chemistry Special Publications, vol. 318, pp. 159–166. Royal Society of Chemistry, Cambridge (2009)

Brunauer, S., Emmett, P.H., Teller, E.: Adsorption of gases in multimolecular layers. J. Am. Chem. Soc. **60**, 309–319 (1938)

Bulushev, D.A., Yuranov, I., Suvorova, E.I., Buffat, P.A., Kiwi-Minsker, L.: Highly dispersed gold on activated carbon fibers for low-temperature CO oxidation. J. Catal. **224**(1), 8–17 (2004)

Cal, M.P., Rood, M.J., Larson, S.M.: Gas phase adsorption of volatile organic compounds and water vapor on activated carbon cloth. Energy Fuels **11**(2), 311–315 (1997)

Carrott, P.J.M., Roberts, R.A., Sing, K.S.W.: Adsorption of nitrogen by porous and nonporous carbons. Carbon **25**(1), 59–68 (1987)

Choung, J.H., Lee, Y.W., Choi, D.K., Kim, S.H.: Adsorption equilibria of toluene on polymeric adsorbents. J. Chem. Eng. Data **46**(4), 954–958 (2001)

Das, D., Gaur, V., Verma, N.: Removal of volatile organic compound by activated carbon fiber. Carbon **42**(14), 2949–2962 (2004)

Datka, J.: Adsorption of benzene and toluene on y-zeolites studied by infrared-spectroscopy. J. Chem. Soc. **77**, 511–517 (1981)

Dimotakis, E.D., Cal, M.P., Economy, J., Rood, M.J., Larson, S.M.: Chemically treated activated carbon cloths for removal of volatile organic carbons from gas streams—evidence for enhanced physical adsorption. Environ. Sci. Technol. **29**(7), 1876–1880 (1995)

El-Sayed, Y., Bandosz, T.J.: A study of acetaldehyde adsorption on activated carbons. J. Colloid Interface Sci. **242**(1), 44–51 (2001)

Figueiredo, J.L., Pereira, M.F.R., Freitas, M.M.A., Orfao, J.J.M.: Modification of the surface chemistry of activated carbons. Carbon **37**(9), 1379–1389 (1999)

Foster, K.L., Fuerman, R.G., Economy, J., Larson, S.M., Rood, M.J.: Adsorption characteristics of trace volatile organic-compounds in gas streams onto activated carbon-fibers. Chem. Mater. **4**(5), 1068–1073 (1992)

Fournel, L., Mocho, P., Brown, R., Le Cloirec, P.: Modeling breakthrough curves of volatile organic compounds on activated carbon fibers. Adsorpt. **16**(3), 147–153 (2010)

Hayashi, T., Kumita, M., Otani, Y.: Degradation of acetaldehyde adsorption performance of impregnated activated carbons. Kag. Kog. Ronbunshu **32**(1), 72–78 (2006)

Hernandez, M.A., Velasco, J.A., Asomoza, M., Solis, S., Rojas, F., Lara, V.H.: Adsorption of benzene, toluene, and p-xylene on microporous SiO₂. Ind. Eng. Chem. Res. **43**(7), 1779–1787 (2004)

Huang, Q.L., Vinh-Thang, H., Malekian, A., Eic, M., Trong-On, D., Kaliaguine, S.: Adsorption of n-heptane, toluene and o-xylene on mesoporous UL-ZSM5 materials. Microporous Mesoporous Mater. **87**(3), 224–234 (2006)

Li, X.Y., Zhu, Z.R., Zhao, Q.D., Wang, L.: Photocatalytic degradation of gaseous toluene over ZnAl₂O₄ prepared by different methods: a comparative study. J. Hazard. Mater. **186**(2–3), 2089–2096 (2011)

Lillo-Rodenas, M.A., Cazorla-Amoros, D., Linares-Solano, A.: Behaviour of activated carbons with different pore size distributions and surface oxygen groups for benzene and toluene adsorption at low concentrations. Carbon **43**(8), 1758–1767 (2005)

Lillo-Rodenas, M.A., Cazorla-Amoros, D., Linares-Solano, A.: Benzene and toluene adsorption at low concentration on activated carbon fibres. Adsorpt. **17**(3), 473–481 (2011)

Mangun, C.L., Daley, M.A., Braatz, R.D., Economy, J.: Effect of pore size on adsorption of hydrocarbons in phenolic-based activated carbon fibers. Carbon **36**(1–2), 123–129 (1998)

Mo, J.H., Zhang, Y.P., Xu, Q.J., Lamson, J.J., Zhao, R.Y.: Photocatalytic purification of volatile organic compounds in indoor

air: a literature review. Atmos. Environ. **43**(14), 2229–2246 (2009)

Mohan, N., Kannan, G.K., Upendra, S., Subha, R., Kumar, N.S.: Breakthrough of toluene vapours in granular activated carbon filled packed bed reactor. J. Hazard. Mater. **168**(2–3), 777–781 (2009)

Okubo, M., Yamamoto, T., Kuroki, T., Fukumoto, H.: Electric air cleaner composed of nonthermal plasma reactor and electrostatic precipitator. IEEE Trans. Ind. Appl. **37**(5), 1505–1511 (2001)

Park, K.H., Shim, W.G., Shon, H.K., Lee, S.G., Ngo, H.H., Vigneswaran, S., Moon, H.: Adsorption characteristics of acetaldehyde on activated carbons prepared from corn-based biomass precursor. Sep. Sci. Technol. **45**(8), 1084–1091 (2010)

Park, S.W., Choi, B.S., Lee, J.W.: Breakthrough data analysis of adsorption of toluene vapor in a fixed-bed of granular activated carbon. Sep. Sci. Technol. **42**(10), 2221–2233 (2007)

Pei, J., Zhang, J.S.S.: Determination of adsorption isotherm and diffusion coefficient of toluene on activated carbon at low concentrations. Build. Environ. **48**, 66–76 (2012)

Piccot, S.D., Watson, J.J., Jones, J.W.: A global inventory of volatile organic-compound emissions from anthropogenic sources. J. Geophys. Res. Atmos. **97**(D9), 9897–9912 (1992)

Popescu, M., Joly, J.P., Carre, J., Danatoiu, C.: Dynamical adsorption and temperature-programmed desorption of VOCs (toluene, butyl acetate and butanol) on activated carbons. Carbon **41**(4), 739–748 (2003)

Pradhan, B.K., Sandle, N.K.: Effect of different oxidizing agent treatments on the surface properties of activated carbons. Carbon **37**(8), 1323–1332 (1999)

Romero-Anaya, A.J., Lillo-Rodenas, M.A., Linares-Solano, A.: Spherical activated carbons for low concentration toluene adsorption. Carbon **48**(9), 2625–2633 (2010)

Rouquerol, F., Rouquerol, J., Sing, K.S.W.: Adsorption by Powders and Porous Solids : Principles, Methodology and Applications. Academic Press, San Diego (1999)

Ruddy, E.N., Carroll, L.A.: Select the best VOC control strategy. Chem. Eng. Prog. **89**(7), 28–35 (1993)

Ruhl, M.J.: Recover VOCs via adsorption on activated carbon. Chem. Eng. Prog. **89**(7), 37–41 (1993)

Salame, I.I., Bandosz, T.J.: Study of water adsorption on activated carbons with different degrees of surface oxidation. J. Colloid Interface Sci. **210**(2), 367–374 (1999)

Sing, K.S.W.: Empirical method for analysis of adsorption isotherms. Chem. Ind. **44**, 1520 (1968)

Sing, K.S.W., Everett, D.H., Haul, R.A.W., Moscou, L., Pierotti, R.A., Rouquerol, J., Siemieniewska, T.: Reporting physisorption data for gas solid systems with special reference to the determination of surface-area and porosity (recommendations 1984). Pure Appl. Chem. **57**(4), 603–619 (1985)

Singh, K.P., Mohan, D., Tandon, G.S., Gupta, G.S.D.: Vapor-phase adsorption of hexane and benzene on activated carbon fabric cloth: equilibria and rate studies. Ind. Eng. Chem. Res. **41**(10), 2480–2486 (2002)

Tamaru, K.: Adsoprtion measurements during surface catalyis. Adv. Catal. **15**, 65–96 (1964)

Tancrede, M., Wilson, R., Zeise, L., Crouch, E.A.C.: The carcinogenic risk of some organic vapors indoors—a theoretical survey. Atmos. Environ. **21**(10), 2187–2205 (1987)

Wagner, C., Hauffe, K.: Examinations of the stationary condition of catalysts in heterogenous reactions I. Zeitschrift Fur Elektrochemie Und Angewandte Physikalische Chemie **44**, 172–178 (1938)

Wagner, C., Hauffe, K.: Analyses concerning the stationary position on catalysts in heterogenous reactions II. Zeitschrift Fur Elektrochemie Und Angewandte Physikalische Chemie **45**, 409–425 (1939)

Wu, C.F., Wu, S.Y., Wu, Y.H., Cullen, A.C., Larson, T.V., Williamson, J., Liu, L.J.S.: Cancer risk assessment of selected hazardous air pollutants in Seattle. Environ. Int. **35**(3), 516–522 (2009)